Australian Journal of Crop Science AJCS

AJCS 14(08):1242-1251 (2020) ISSN:1835-2707
doi: 10.21475/ajcs.20.14.08.p2287

Integration of UAV data with soil water balance models for evaluation/monitoring of maize water stress

Alimonti Claudio[1], Baiocchi Valerio[2*], Spadaro Carlo[2], Spadaro Raffaele[1]

[1]DICMA, Sapienza University of Rome, I-00184 Rome, Italy
[2]Department of Civil, Constructional and Environmental Engineeering (DICEA), Sapienza University of Rome, I-00184 Rome, Italy

***Corresponding author: valerio.baiocchi@uniroma1.it**

Abstract

UAV based photogrammetry and 3D mapping are gaining fast and wide applications around the world majorly due to the relatively low-cost advantage it offers in the acquisition of high resolution multispectral acquisitions, compared to Aerophotogrammetry and satellite acquisitions. This research seeks to demonstrate the applicability of UAV photogrammetry visible, multispectral and thermal in investigating some physiological indexes of plants, reflecting plant physiological traits. A maize field in Latina (Italy) was acquired using a Fly Novex drone and with different cameras for the various acquisitions and consequently for different flight heights. The obtained images were processed using different photogrammetric models and a variable number of Ground Control Points (GCPs) for the georeferencing and accuracy assessment as well. Subsequently, by combining hydrological simulation methods and the use of physical indicators of the state of water stress, a method is proposed for predicting crop water consumption. The study conducted on the agricultural land of test site has provided useful results in terms of water savings, with an estimated value of three quarters of the total cubic meters of water needed to bring the land to saturation.

Keywords: UAV, remote sensing, water stress, multispectral images, thermal images, water balance models, maize.

Introduction

The limited availability of water resources is a factor of increasing importance for world agriculture, which is most acute in periods of heavy rainfall. Even countries with good water availability are still encountered the irregularities of rainy events, as water demand from all the main activities continues to increase. As a result, the amount of water in soils is in many cases exceptionally low and insufficient to provide a water reserve for crop development. For these reasons, the saving and the careful use of water resources used in agricultural practices are increasingly of interest to the world of research. Currently, there is a growing development of systems to support irrigation programming and to monitor crop water consumption in real time or at frequent intervals. In this context, technologies based on Unmanned Aerial Vehicles (UAV) compared to conventional platforms (Baiocchi et al., 2017a; Palazzo et al., 2012), offers the possibility of obtaining more detailed information in a very short time (Turner at al., 2011; Alicandro M, 2018; Lo Brutto M, 2018; Panigada at al., 2014; Rossini at al., 2013). In recent years, several studies have highlighted the presence of a strong correlation between some of the main physiological indexes of the plant and others obtained by interpreting remote sensed images. Vegetational indexes (VIs), obtained from thermal and multispectral tele-detected data, can be used to describe the water status of plants, as reported in numerous studies in literature (Suarez at al., 2009; Chapman at al., 2014; Garcia-Ruiz at al., 2012; Gago at al., 2015; Zarco-Tejada at al., 2011; Kendal & De Jonge, 2015; Zhuang at al., 2014). From reflectance information in the different ranges of the electromagnetic spectrum, stress conditions can be prevented before the effects are visible. This allows timely intervention with water supplies, avoiding compromising crop productivity. Water stress arises when the plant's water demand exceeds its real availability in the soil, which leads to stomata closure, leading to a reduction in the rate of transpiration, resulting in an increase in the temperature of the leaf layer. For this reason, thermal images of the plant cover can provide information on the rate of instantaneous transpiration at the acquisition date, allowing the detection of plant stress. The factor that limits the use of thermal chambers for stress detection is the absence of high-resolution spatial thermal sensors due to the technological limits to distinguish them. The integration of high-resolution optical and multispectral images allows the full potential of each sensor type to be exploited. Plant cover temperature (T_C) has been proposed to track the variation in leaf potential (l) as a consequence of increased or decreased water availability due to the change in level in the soil layer explored by the roots (Wayne and Blizzard, 1980). In the past, several studies have investigated the relationships between water potentials that occur at every level of the continuous Soil-Plant-Atmosphere Continuum system (SPAC) (Newman, 1969; Hunt Jr., 1991). These studies

have shown that the flow within the SPAC system can be designed in analogy to an electrical circuit. Based on these hypotheses, it is possible to characterize the variation of the water content at each level of the system and; therefore, to plan irrigation interventions, reducing water waste and plant stress. This study aims to assess the potential of using thermal and multispectral UAV images to detect the occurrence of stress in a maize field in a preventive manner.
The specific objectives of this work are oriented towards: (i) evaluate the plano-altimetric accuracy obtainable from these images (ii) map the water stress of the area from UAV thermal data; (iii) analyze the relationship between the T_C temperature computed by the FLIR chamber, and the physiological and hydraulic properties of the area of interest; (iv) evaluate a new water balance model for irrigation planning, based on the integration of UAV data into traditional irrigation support systems.

Results and discussion

Particle size tests and the SWRC curve

Two particle sizes were analysed from the soil sample using different series of sieves (Fig. 4). From the analysis, the characteristic parameters for the dimensional classification and for the theoretical reconstruction of the water retention curve are extrapolated by linear interpolation (Fig. 5).
Between the two curves, curve B was selected as representative of the entire area, since it was only possible for the latter to obtain the useful parameters. About 60% of the curve feedthrough falls within the dimensional range of sand, while 40% falls within the gravel range. According to the AGI 1977 classification, the sample is a gravelly sand. By knowing the D_{10} and the slope of the particle size curve, the water retention curve was drawn thanks to the results obtained by Fredlund (2007). As it is impossible to carry out an extended soil data collection campaign, the result is a single Soil Water Retention Curve (SWRC). This makes it impossible to take into account the spatial variability of the hydraulic characteristics of the area; and therefore, makes the localized and punctual analysis of water flows and consequently of irrigation supplies not very meaningful. However, the large-scale analysis and the related assessment of the required water supply remains valid.

Water stress maps

In order to assess the presence of water stress in the area, thematic maps have been used to represent the distribution of the values assumed by the CWSI, DANS and DACT indices (Figure 6 a,b,c). These indexes use the temperature value of the plant cover T_c as the main data for the evaluation, generally assumed as a single value and representative of the peak condition reached in a day. The values of the indexes have been divided into 5 intervals with colour variations from green to red where the stress condition is at its highest. As can be seen, particularly through the DACT index, there are rather high temperature differences over the whole area, compared to the minimum stress condition. The whole field was under stress, as the soil was not irrigated for several days because the maize was close to the harvest time. In the maps, the presence of a more stressed area justified by the presence of dwellings in that area, involving an additional source of heat. The NDVI map (Figure 6d) allows detailed discrimination between vegetation and non-vegetative areas. In this context, the index could be used, both as a source of health information and as a support for image segmentation to derive useful data on plants only, excluding soil and shaded areas. In the specific case of maize, the architecture of the plant cover is such that it does not compromise classification, as the distance between the individual plants is about 70 cm. The results obtained from the temperature maps and the NDVI index, provide similar results in terms of water stress.

The initial moisture profile

From the T_C temperature data (equation 4), it was possible to obtain a spatial distribution of the values of the leaf potential ψ_l for the whole area of interest. At the acquisition date, the hypothesis was made that the entire area was in a condition of suboptimal humidity (maximum water stress K_s=0). This hypothesis is justified because: (i) the temperatures in the period prior to the acquisition date were such as to generate significant water losses through evapotranspiration (ET_c=3.06 mm/day); (ii) the land was not irrigated during the same period. According to the FAO method, under maximum stress conditions, T is equal to 0, and applying the stationary flow model (9), we obtain $\psi_s=\psi_l$, with values for the whole area constantly below the flash-off point (ψ_{max}=40.1 bar; ψ_{min}=20.9 bar). The humidity map (Figure 7) is in line with the results obtained from the stress analysis. In fact, the areas most at risk are characterized by reduced humidity levels of about 3% (a value that, for an average sand, is between the point of withering and the hygroscopic level).
The profiles obtained suggest restoring the soil to humidity levels close to the field water capacity, with an average volume contribution of $43*10^{-3}$ m^3/m^2.

Irrigated management

The values of the hydrological constants CC and PA obtained from FAO Book 56, with reference to the grain size class of sand, are 0.12 m^3/m^3 and 0.045 m^3/m^3, respectively. In the specific case of maize, the soil thickness to be humidified was 70 cm. The coefficient of performance of the irrigation system shall be considered to be a value of 0.7.
In Figure 8, we compare the ET_c and ET_r values useful to identify the stress phases that correspond in Figure 9 to the various phases, in which it is necessary to intervene with irrigation. Based on the results obtained and observations made in the field, the water saving of about 70% are estimated, compared to the operating conditions, which are usually carried out by the operator in the area.

Materials and Methods

Study area

The study area is located near the city of Latina (Italy) between the hamlet of Tor tre Ponti and the municipality of Borgo Faiti along the "Via Falchetto" Road (41°29'50"N, 12°57'10"E, WGS84) and includes about 2.6 ha of *Zea mays* (or sweet corn) with about 120 days (number of days after sowing, which is required for collection). They were planted in the first half of June 2017 (Figure 1).

Table 1. Weather data for the LIRL station at Latina Airport for the period between the acquisition date and the stamping phase. T_{max} and T_{min} are maximum and minimum average daily air temperature at 2 m height expressed in degrees centigrade, RH_{max} and RH_{min} are relative humidity, z is the height, u_2 is the wind speed at 2 m height m⁄s.

Data	T_{max} (°C)	T_{min} (°C)	RH_{max} (%)	RH_{min} (%)	z(m)	u_2(m/s)
19/10/2017	23	13	100	60.7	1.3	3.40
20/10/2017	25	12	100	47.3	1.3	4.53
*21/10/2017	26	14	90	50	1.3	5.21
*22/10/2017	22	13	95	40	1.3	7.69
23/10/2017	21	12	87.6	28.4	1.3	9.07
24/10/2017	25	14	41.1	20.7	1.3	6.80
25/10/2017	23	10	71.8	30.8	1.3	4.53
26/10/2017	24	11	87.5	11	1.3	3.98
27/10/2017	22	8	100	60.5	1.3	3.98
*28/10/2017	20	9	88	60	1.3	5.09
*29/10/2017	24	10	92	43	1.3	6.68
30/10/2017	20	8	100	52.5	1.3	7.38
31/10/2017	22	11	93.6	35.4	1.3	3.98

[1] The values marked with an asterisk are hypothesized due to the absence of weather data.

Fig 1. In red, the area subject to thermal acquisition is highlighted, red area is approximately 360 meters long.

Table 2. Kcb values corrected for each fundamental phase of phenological development.

u_2 (m/s)	RH_{min} (%)	h (m)	$K_{cb, ini}$	$K_{cb, mid}$	$K_{cb, end}$
2.64	46.78	1.5	0.150	1.102	1.002

Fig 2. UAV exacopter, model: Novex, brand “IDS”with Sony Ilce 6000 camera.

Fig 3. Multispectral camera, brand: "Tetracam".

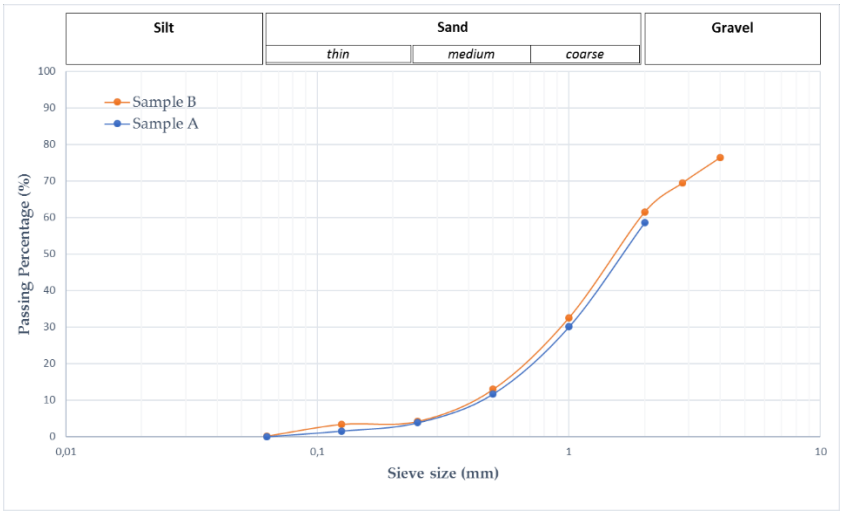

Fig 4. Grain size curves of the two soil samples A and B, weighing 496.72 g and 600 g, respectively. For sample B, also the 283 mm and 4 mm sieve.

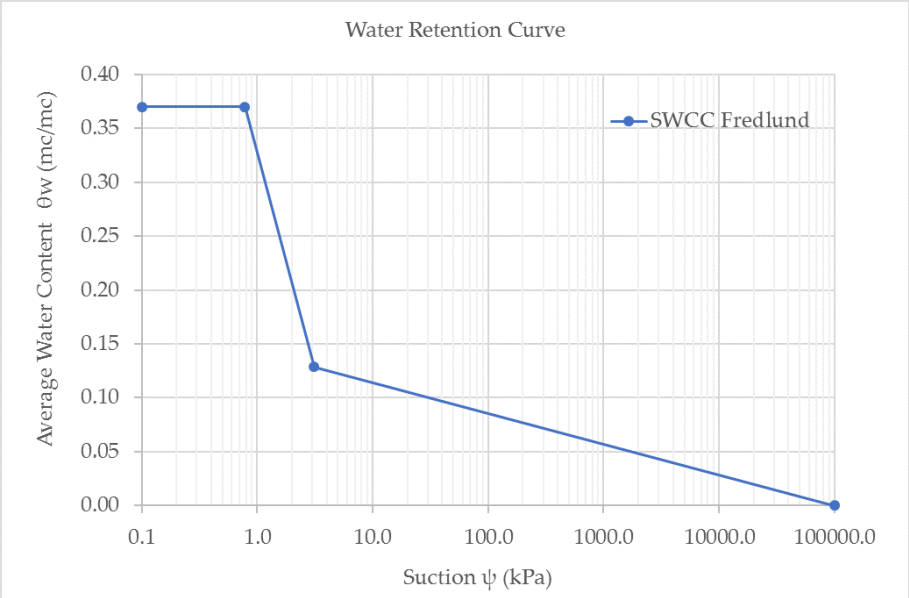

Fig 5. Soil curve (model based on Fredlund theory), which describes the relationship between the water content in the soil pores and the matrix potential.

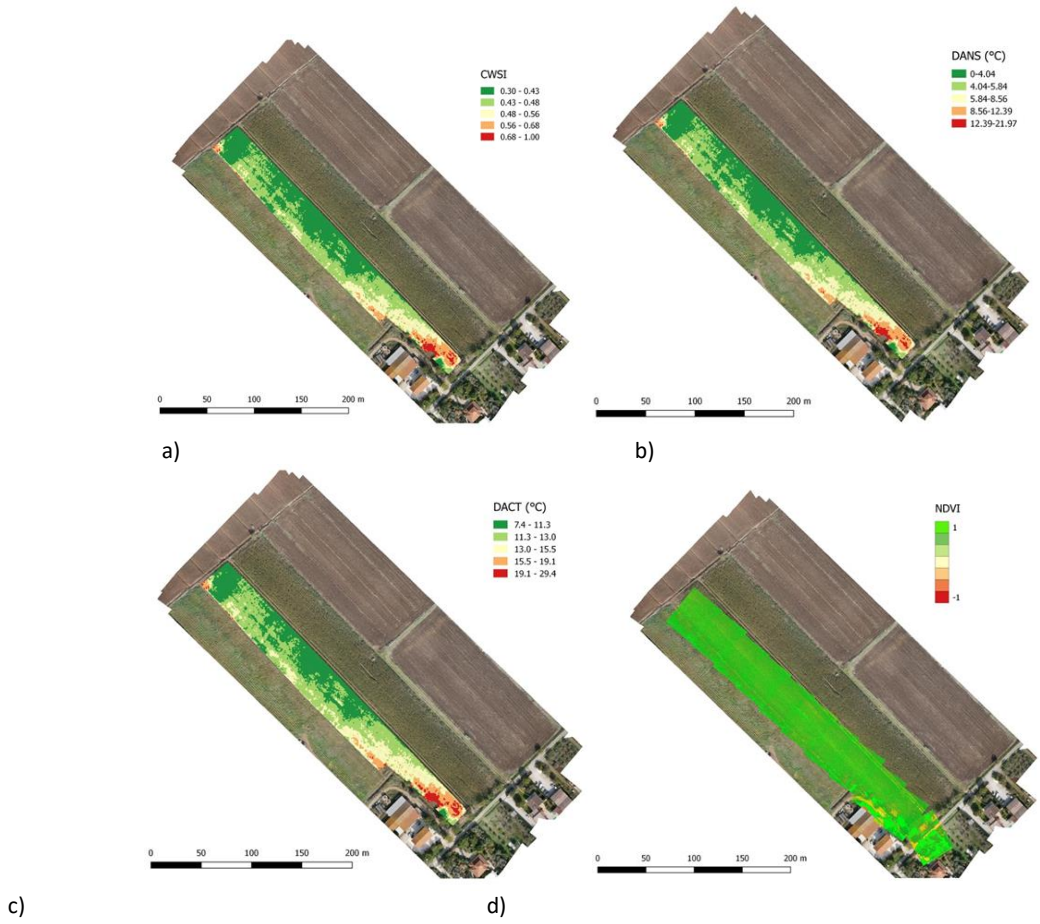

Fig 6. Discrete colors representation of spatial distribution of the different water stress indexes, (a) CWSI; (b) DANS; (c) DACT; (d) NDVI; as extrapolated from the images.

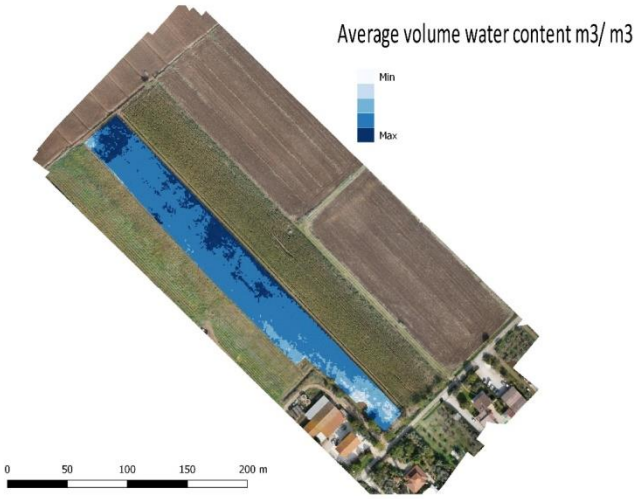

Fig 7. Humidity profile map at acquisition date (20/10/2017).

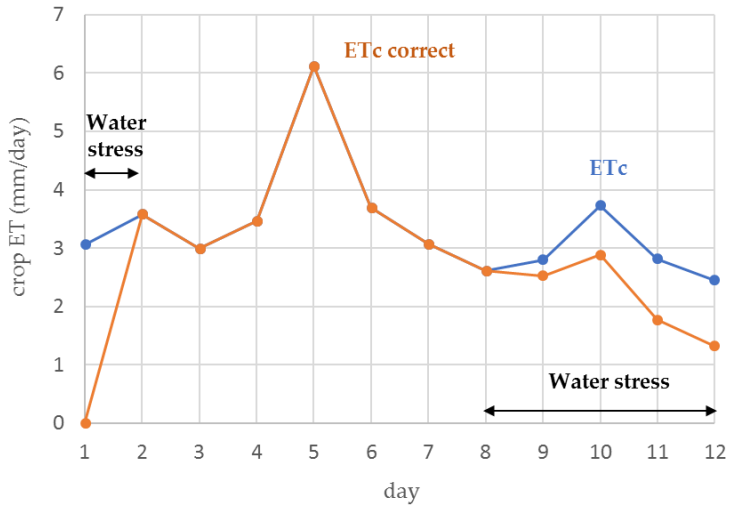

Fig 8. Programming of interventions without waste and without water stress.

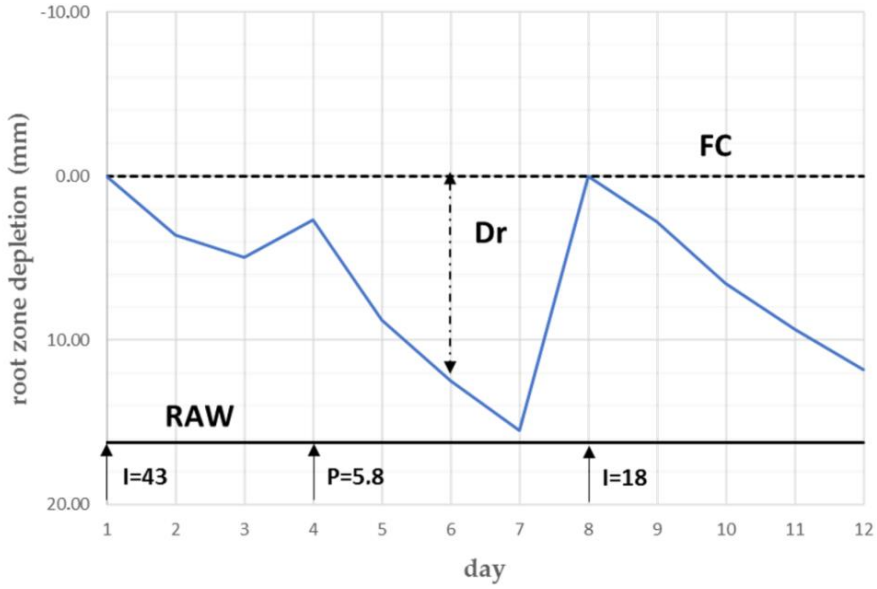

Fig 9. Comparison of ET_C and ET_r. The water stress phases identified by the ET_r<ET_C condition.

Plant materials

The maize was irrigated by sprinkling the soil for a total of 11 repetitions, from June to the first half of September, with volumes that bring saturation to the soil at each intervention. The acquisition campaign took place in the second half of October, when the plants reached full maturity (close to harvest). The choice fell on this period, for either technical and organizational reasons or critical stages of maize growth that are the vegetative phase and especially the flowering.

Weather data

The reference weather data for the area were obtained from historical data recorded by the LIRL station of the Latina Scalo (Italy) military airport, located near the area under study. This data was collected over a period from the acquisition date to the date of harvest, when maize is less sensitive to water stress.

Soil data collection

From the area, a soil sample was taken for particle size analysis by sieving to obtain particel size distribution.

Statistical analysis

Starting from the characteristic parameters of the particle size distribution (D_{10} and slope of the curve), the soil can be characterised from a hydraulic point of view, by assuming its homogeneity to the area. It is possible to reconstruct the water retention curve, using the theoretical model of Fredlund. The equations of the Fredlund model was used as input variables: the residual suction value, saturated soil volume content, and residual water content. These parameters allow identifying the three characteristic zones of the drainage curve, useful to determine the initial humidity profile and then implement the hydrological simulation models for a specific reference period.

Optical, thermal and multispectral imaging and processing techniques

The acquisition was carried out on October 20, 2017, during which three distinct flights were conducted between 11:00 am and 13:30 am using an exacopter (6 motors) model "Novex" built by "Ingegneria dei Sistemi" Company (IDS, 2019) (Figure 2).

Visible images flight

The first flight was conducted by equipping the drone with a digital camera SONY ILCE α6000 with a focal length of 16mm and FOV 23.5 x 15.6 mm operating in the visible (Sony, 2019). Ninety-three images of the area were taken with this camera at an average flight altitude of about 95 m above ground level. For the planning of the flight, an along track overlap of 80% and an across track overlap of 45% were respected. These overlap values are suggested by the planning software (Pix4D Ctrl+) and have been successfully tested in previous experiments.

Multispectral images flight

The second flight was carried out with a TETRACAM ADC Snap multispectral camera on board with sensors capable of detecting the range of the visible and near infrared (3 Green, Red, NIR bands equivalent to Landsat TM2, TM3, TM4) in a range between 520-920 nm (Tetracam, 2019) (Fig.3). In this case, 20 images of the area were acquired at an average height of about 125 m.

Thermal images flight

The last flight was conducted with a FLIR VUE PRO R thermal imaging camera on board with 9mm (35° x 27°) focal length and resolution of 336 x 256 pixels and a wavelength range of 7-13.5 μm (FLIR, 2019), with which 71 photos were taken at a flight altitude of about 90 m.

Images processing

The optical images acquired were imported into the Agisoft Photoscan software (1.4.1) for geometric processing. The orientation of the frames in this software is based on the structure from motion (SfM) (Ullman, 1979; Turner at al., 2012; Ialongo, 2016) technique for the reconstruction of the mosaic and the digital terrain elevation model (DEM). The software can operate without ground control points (GCPs), basing the external orientation of the model only on the coordinates obtained by the navigation system (GPS+ IMU) of the drone that works in point positioning; and therefore with plano-altimetric accuracy insufficient for proper mapping (Baiocchi at al., 2014; Baiocchi at al., 2017b; Caroti at al., 2015; Costantino & Angelini, 2012). For this reason, a differential GPS/GNSS measurement campaign was performed in Post Processing and RTK (Real Time Kinematic) mode with TOPCON "Legacy E" Receiver referred to the network of permanent stations managed by the Lazio Region and framed in the ETRF2000-RDN reference system (Regione Lazio, 2019). The processing of thermal and multispectral images involved a small portion of the entire area, with an extension of about 1 ha. In the configuration, the navigation system was not fully interfaced with the multispectral and thermal cameras; and therefore it was not possible to associate (with certainty) the navigation parameters to the single images. For this reason, and due to the smaller overlap between each frame of multispectral and thermal capture, it was not possible to process these images in the AgiSoft Photoscan environment. Therefore, the orthomosaics were created within the PCI Geomatics 2014 environment, using the rigorous photogrammetric model for thermal images and rational polynomial models for multispectral models. For these last two applications, the GCPs previously used on optics have often proved to be unidentifiable. For this reason, others GCPs have been acquired by extrapolating the coordinates of some recognizable points directly on the optical mosaic previously generated. This solution is correct due to the higher resolution and consequent accuracy of the optical image compared to multispectral and thermal.

In this case, the orthorectification required the availability of a DEM which could not be obtained from the cartography because of the small slope of the area; and therefore, the reduced number of contour lines. For this reason, a portion of DEM acquired by airborne Lidar was used. This DEM was made available by the Ministry of the Environment (Geoportale Nazionale, 2019).

With regard to thermal image processing, the temperature values of the plant cover (Tc) were averaged and extracted for an area of 6X6 pixels (1 m^2), using FlirTools and eCognition Development 9 software. Based on thermal indices, the water stress indexes were calculated, such as CWSI (Crop Water Stress Index), DANS (Degrees Above Non-Stessed Canopy) and DACT (Degrees Above Critical Temperature):

$$CWSI = (dT_m - dT_{LL}) / (dT_{UL} - dT_{LL}), \quad (1)$$

$$DANS(H) = T_C(h) - T_C\,NS(h), \quad (2)$$

$$DACT(H) = \max[0, T_C(h) - T\,\mathrm{critical}], \quad (3)$$

In addition to the thermal indexes, the leaf potential (ψ_f) was calculated by using the linear equation of statistical regression that binds this index to the temperature value T_C. Equation (4) is the result of a trial conducted on a maize field in northern Colorado, during which T_C values obtained from a thermal imaging camera and ψl the leaf potential was measured in situ (Kendal and De Jonge, 2015).

$$T_C = 1.1423 \cdot \psi_l + 11.556, \quad (4)$$

The temperature value is expressed in centigrade degree, while the leaf potential in bar. An acceptable correlation index (R^2= 0.895) was found in the test.

The Normalized Difference Vegetation Index (NDVI) of the area was extrapolated from the multispectral images using the PixelWrench2 software. This indicator assesses the presence of photosynthetic activity, as it relates the red spectrum, where there is absorption by chlorophyll, and the near-infrared spectrum, where leaves reflect light to avoid overheating. NDVI is a good indicator of stress, since under such conditions the plant reduces its photosynthetic activity by decreasing the index value.

Weather data collection and processing

Currently, remote sensing techniques combined with hydrological simulation methods are used for irrigation planning. These applications allow the assessment and quantification of crop water consumption, expressed as the total amount of water to be resupply into the soil by irrigation. The simplified expression of the balance sheet equation is shown below.

$$I=ET_r - P/r, \quad (5)$$

The terms of exchange with the water table (infiltration) and run-off are not present, since irrigation is carried out in the summer period, characterized by often negligible water table contributions, while the efficient irrigation system should not allow losses due to run-off and drainage.

The term I refers to irrigation, ET_r to reference (or specific) evapotranspiration, with P to precipitation and with r to the coefficient of performance of the system. The FAO method (Allen et al, 1998) was used to estimate the evapotranspiration rate, using the Penmann-Monteith equation as the standard for assessing the evapotranspirational demand for reference atmosphere (ET_0).

$$ET_0 = \frac{0.408\,\Delta\,(R_n - G) + \gamma \frac{900}{T+273} u_2\,(e_s - e_a)}{\Delta + \gamma(1 + 0.342\,u_2)} \quad (6)$$

Where;

ET_0=reference evapotranspiration mm⁄d;

R_n=net radiation to the crop area MJ⁄(m^2 d);

G=heat flow in the ground MJ⁄(m^2 d);

T= average daily air temperature at 2 m height (°C);

u_2=wind speed at 2 m height m⁄s;

es = vapour pressure kPa;

e_a=air vapour pressure kPa;

Δ=slope of the curve expressing the saturated vapour pressure as a function of the temperature kPa⁄(°C);

γ=psychrometric constant kPa⁄(°C).

Known the weather and climate variables (e.g. temperature, humidity, wind speed, etc.), all other quantities can be calculated according to these by following the steps described in the FAO56 notebook.

The table below shows the main meteorological parameters taken from the LIRL station at Latina Airport (Table 1).

The double cultivation coefficient approach was applied to the evaluation of crop evapotranspiration. This method allows the cultivation coefficient K_c to be divided into two distinct terms, soil evaporation and plant transpiration. The K_c coefficient incorporates and synthesizes all the effects on evapotranspiration, linked to the morpho-physiological characteristics of each crop and to the phenological phase of study.

$$ET_C = (K_{cb} + K_e) \cdot ET_0, \quad (7)$$

ET_C: crop evapotranspiration (or potential);

Kc_b: transpiration coefficient;

K_e: evaporation coefficient.

Equation 7 is provided by the FAO-56 notebook for calculating the coefficient K_c and is known as the double culture coefficient approach, which involves the splitting of the K_c into two distinct terms that separately describe the evaporation contribution of the soil (K_e) and transpiration of cultures (K_{cb}). However, FAO-56 provides the values of K_c for different crop species, although these values are only an indication and must be combined with inspections, interviews with farmers and further experiments. Below is just the procedure for calculating the transpiration component $K_{cb}\,E_{T0}$ given that at the time of the air acquisition campaign, the corn crop had already reached full maturity.

$$K_{cb} = K_{cb\,(Tab)} + [0.04(u_2 - 2) - 0.004(RH_{min} - 45)]\left(\frac{h}{3}\right)^{0.3} \quad (8)$$

K_{cb} ($_{Tab}$) = the value of K_{cb} mid or K_{cb} end if ≥0.45 taken from Table 17 of FAO-56;

u_2 = the average daily value of the wind speed at 2 m height from the ground during the intermediate (mid) and ripening (end) stages for 1 m/s ≤ u_2 ≤ 6 m/s

RH_{min} = the average daily value of relative minimum humidity during the intermediate (mid) development and maturation phases (end) for 20% ≤ RH_{min} ≤ 80%;

h = average plant height (m) during the intermediate (mid) and ripening (end) phases provided in Table 12 (FAO-56) for 20% ≤ RH_{min} ≤ 80%.

The FAO method also allows real evapotranspiration to be calculated by adding an additional coefficient of K_s (coefficient of water stress). This approach reduces the evapotranspiration rate when the soil is not at optimal moisture conditions for crop development. The coefficient K_s is determined through the continuous updating of the water balance by the equation:

$$K_s = (RU - D_r) / (RU - RFU), \quad (9)$$

Where; usable water reserve is RU, easily usable reserve is RFU and D_r the term water scarcity relative to FC field capacity.

Calculation of suction capacity

The driving force of the water flow within the plant is the gradient of water potential between the soil and the atmosphere. In this path, the water meets a series of resistances. Van den Honert suggested that this flow should be conceived as a series of resistors. To characterize the variation of the water content in the liquid state, at each level of the plant, a mass balance can be used, known as the incoming and outgoing flow terms. Moreover, water accumulations are considered null. It follows that the flow of water that transpires is equal to the radical absorption.

$$T = \frac{\psi_s - \psi_l}{R_{total}}, \quad (10)$$

In equation (10), the transpiration rate is indicated by T, ψ_s the suction potential ψs the leaf potential and the total resistance offered by the whole SPAC system is indicated by R_{tot}.

This approach is called Van den Honert's stationary flow model, which allows characterizing the flows and components of the entire soil-plant-atmosphere system in analogy to an electrical circuit.

Specific volume of water and time of irrigation intervention

To determine the amount of water needed to rationally ensure the water reserve useful for crop development, it is necessary to establish the soil layer to be humified in relation to the depth, where the maximum capacity for root extraction is found. In addition, definition of the values of hydrological

constants such as field capacity (CC) and point of withering (PA) is vital. By knowing the values of CC and PA you can identify the irrigation intervention point that divides the useful reserve RU into two parts: (i) the reserve easily usable (RFU), (ii) the critical limit of humidity (LFU). These values depend heavily on the extraction capacity of each type of crop. The calculation of the specific volume of water is referred to a parcel of soil with dimensions V(m^3) and a percentage of humidity equal to U, equation:

$$V = (CC - U) * V, \quad (11)$$

Thus, the volume of calculated water should be increased by taking into account the efficiency of the irrigation system. The irrigation coefficient of performance (r) can be considered as 0.7 for sprinkler irrigation systems or 0.9 for micro irrigation systems. The moment of irrigation intervention is determined by a continuous updating of the water balance expressed in terms of water exhaustion D_r. The term D_r increases when there are losses due to evapotranspiration up to a maximum value at the critical limit of humidity, which means that it is necessary to intervene with irrigation because all the easily usable reserve has been exhausted.

$$D_{r,i} = D_{r-i} + ET_r - P/r, \quad (12)$$

Conclusions

The first objective of this work was to evaluate the geometric accuracy of the images to map the water stress status of a cultivated area, starting from the interpretation of images taken by a UAV. The optical images were processed using SFM to obtain planoaltimetric accuracies of 30 cm with the ortho images and 80 cm with the DEM. The biggest differences are in areas with plantations and trees, since with the DEM it is not possible to penetrate crops. Therefore, it is not possible to evaluate the accuracy with certainty. It can be said that with a reference lidar, the use of the drone with the DEM can be used to measure the height of crops. The lower resolution can cause the lack of certain navigational data and the reduced overlap of the frames. In the case that thermal and multispectral have not allowed to exploit SfM orientation and reconstruction techniques, the most laborious rigorous photogrammetric and strict Rational Polinomial Function model respectively are used. The altimetric accuracies achieved in this case were in the order of 70 cm for thermal images and 40 cm for multispectral ones. To maximise the potential of UAV technology for environmental and agricultural applications, it is essential to develop an automated, efficient and accurate technique for orthorectifing and generating mosaics from the large number of images available. The goal is to always apply automatic algorithms such as the SfM for all images to obtain the temperature and multispectral information for larger areas more quickly and accurately. Therefore, it is considered useful in the future to develop methodologies to interface navigation data to individual images. An open problem remains that of collimate with known coordinate points on thermal images where classic geometric details are often difficult to see. Another solution could be to install a thermal and optical camera together on the aircraft so that the orientation of the optical images can allow the thermal to be oriented simultaneously, taking into account the relative orientation between the two sensors.

By combining hydrological simulation methods and physical indicators of the state of water stress, the aim was to propose a method for planning crop water consumption. This application requires more information (density of the root system and maximum length of the roots) and a more detailed soil analysis to estimate the hydraulic conductivity in conditions of saturated and unsaturated soil. The stationary flow model and the FAO method cannot be combined to determine soil suction potential, so the actual breathable flow can only be estimated by a simulation model of the absorption process. The impossibility of generating precise and local estimates of water flows has not allowed the planning of interventions at the scale of the control unit. For this reason, the estimated savings are to be considered in a global way. In fact, the procedure reported in this work can represent a preliminary analysis, due to possibility of establishing the areas to be sampled for the collection of soil data, and saving time and costs for subsequent monitoring. For realization of a service mainly based on the drone plane data, it would be appropriate to evaluate, the possibility of deepening the campaign of collecting data on the field in order to obtain a spatial distribution of the humidity profiles as realistic as possible.

Furthermore, it would be very useful in future campaigns to acquire biometric data on crops in order to link water stress data with the biomass production/growing crop yield map.

However, the study conducted on the agricultural land of the *Tor Tre Ponti* area has produced a satisfactory result in terms of water savings, with an estimated value of three quarters of the total cubic metres of water needed to bring the land to saturation (about 2000 m^3/ha).

Conflicts of Interest: The authors declare no conflict of interest.

References

Baiocchi V, Zottele F, Dominici D (2017a) Remote Sensing of Urban Microclimate Change in L'Aquila City (Italy) after Post-Earthquake Depopulation in an Open Source GIS Environment. Sensor-Basel. 17 404.

Palazzo F, Latini D, Baiocchi V, Del Frate F, Giannone F, Dominici D, Remondiere S (2012) An application of COSMO-SkyMed to coastal erosion studies. Eur J Remote Sens. 45: 361–370.

Turner D, Lucieer A, Watson C (2011) Development of an unmanned aerial vehicle (UAV) for hyper resolution vineyard mapping based on visible, multispectral, and thermal imagery. In: Proceedings of 34th International Symposium on Remote Sensing of Environment. p. 4.

Alicandro M, Dominici D, Buscema PM (2018) A New Enhancement Filtering Approach for the Automatic Vector Conversion of the UAV Photogrammetry Output. In: Ioannides M. et al. (eds) Digital Heritage. Progress in Cultural Heritage: Documentation, Preservation, and Protection. EuroMed 2018. Lecture Notes in Computer Science, vol 11196. Springer, Cham.

Lo Brutto M, Ebolese D, Dardanelli G (2018) 3d modelling of a historical building using close-range photogrammetry and remotely piloted aircraft system (RPAS). Int. Arch. Photogramm. Remote Sens. Spatial Inf. Sci. XLII-2: 599-606, https://doi.org/10.5194/isprs-archives-XLII-2-599-2018.

Panigada M, Rossini M, Meroni M, Cilia C, Busetto L, Amaducci S, Boschetti M, Cogliati S, Picchi V, Pinto F, Marchesi A, Colombo R (2014) Fluorescence, PRI and canopy temperature for water stress detectioning cereal crops. Int J Appl Earth Obs. 30:167-178.

Rossini M, Fava F, Cogliati S , Meroni M, Marchesi M, Panigada C, Giardino C, Busetto L, Migliavacca M, Amaducci S, Colombo R (2013) Assessing canopy PRI from airborne imagery to map water stress in maize. Isprs J PhotogrammI. 86:168–177

Suárez L, Zarco-Tejada P, Gonzalez-dugo V, Berni JAJ, Sagardoy R, Morales F, Fereres E (2010) Detecting water stress effects on fruit quality in orchards with time-series PRI airborne imagery. Remote Sense Environ. 114: 286-298.

Chapman S C, Merz T, Chan A, Jackway P, Hrabar S, Dreccer M F, Holland E, Zheng B, Ling T J, Jimenez-Berni J (2014) Pheno-copter: a low-altitude autonomous remote-sensing robotic helicopter for high-throughput field-based phenotyping. Agronomy. 4:279-301.

García-Ruiz F, Sankaran S, Maja J M, Lee W S, Rasmussen J, Ehsani R (2013) Comparison of two aerial imaging platforms for identification of Huanglongbing-infected citrus trees. Comput Electron Agric. 91: 106-115.

Gago J, Douthe C, Coopman RE, Gallego PP, Ribas-Carbo M, Flexas J, Escalona J, Medrano H (2015) UAVs challenge to assess water stress for sustainable agriculture. Agricultural Water Management. 153:9-19.

Zarco-Tejada PJ, González-Dugo V, Berni JAJ (2011) Fluorescence temperature and narrow-band indices acquired from a UAV platform for water stress detection using a micro-hyperspectral imager and a thermal camera. Remote Sensing of Enviroment. 117:322-337.

Kendal C, De Jonge ST (2015) Comparison of canopy temperature-based water stress indices for maize. Agr Water Manage. 156:51-62.

Zhuang J, Yu GR, Nakayama K (2014) A Series RCL Circuit Theory for Analyzing Non-Steady-State Water Uptake of Maize Plants. Sci Rep. 4: 6720.

Wayne E, Blizzard J S (1980) Comparative Resistance of the Soil and the Plant to Water. Plant Physiol .

Newman E (1969) Resistance to water flow in soil and plant. 1.Soil resistance in relation to amounts of root: Theoretical estimates. J Appl Ecol. 6(1): 1-12.

Hunt Jr. ER, Running SW, Federer CA (1991) Extrapolating plant water flow resistances and capacitances to regional scales. Agr Forest MMeteorol. 54(2-4):169-195.

Fredlund DG, Rahardjo DH (2007) Volume change theory. In: Soil Mechanics for Unsaturated Soils. DOI:10.1002/9780470172759

Ullman S (1979) The interpretation of structure from motion. Proc R Soc Lond. B. 203:405-426.

Turner D, Lucieer A, Watson C (2012) An automated technique for generating georectified mosaics from ultra-high resolution unmanned aerial vehicle (UAV) imagery based on structure from motion (SfM) point clouds. Remote Sens-Basel. 4: 1392-1410.

Ialongo R (2016) Trattamento delle immagini da drone mediante algoritmi fotogrammetrici tradizionali e algoritmi SfM. Graduation thesis at Sapienza University of Rome, Italy.

Baiocchi V, Dominici D, Milone MV, Mormile M (2014) Development of a software to optimize and plan the acquisitions from UAV and a first application in a post-seismic environment. Eur J Remote Sense. 47: 477–253.

Baiocchi V, Giammarresi V, Ialongo R, Piccaro C, Allegra M, Dominici D (2017b) The survey of the Basilica di Collemaggio in L'Aquila with a system of terrestrial imaging and most proven techniques. Eur J Remote Sense. 50(1):237–253.

Caroti G, Martinez-Espejo Zaragoza I, Piemonte A (2015) Accuracy assessment in structure from motion 3D reconstruction from UAV-born images: The influence of the data processing methods. In ISPRS Archives (Eds.) Int Arch Photogramm. doi:10.5194/isprsarchives-XL-1-W4-103-2015.

Costantino D, Angelini M G (2012) Process modeling and photogrammetric production for structural investigations concerning to the collapse of Palazzo Edilizia in Salerno (Italy). In Lecture Notes in Computer Science (including subseries Lecture Notes in Artificial Intelligence and Lecture Notes in Bioinformatics) (Vols. 7616 LNCS pp. 440–448). 4th International Conference on Cultural Heritage EuroMed 2012. Limassol Cyprus. doi:10.1007/978-3-642-34234-9_45

Geoportale nazionale (2019) (www.geoportalenazionale.it) (last seen online: 08/30/2019)

Regione Lazio (2019) http://gnss-regionelazio.dyndns.org/Spiderweb/frmIndex.aspx (last seen online: 06/30/2019)

Allen RG, Pereira L, Raes D, Smith M (1998) Crop evapotranspiration – Guidelines for computing crop water requirements – FAO Irrigation and drainage. https://appgeodb.nancy.inra.fr/biljou/pdf/Allen_FAO1998.pdf (last seen online: 09/03/2019)

IDS (2019) Novex a Short-Range Multi-Rotor Uav. https://www.idscorporation.com/pf/novex/ (last seen online: 08/30/2019)

Sony (2019) Ilce-6000-body-kit. https://www.sony.com/electronics/interchangeable-lens-cameras/ilce-6000-body-kit/specifications (last seen online: 08/30/2019)

Tetracam (2019) ADC Snap. http://www.tetracam.com/Products-ADC_Snap.htm (last seen online: 08/30/2019)

FLIR (2019) FLIR Vue Pro R. https://www.flir.com/products/vue-pro-r/ (last seen online: 08/30/2019)